Hindawi Publishing Corporation
Journal of Nanomaterials
Volume 2014, Article ID 350579, 14 pages
http://dx.doi.org/10.1155/2014/350579

Research Article

In Vitro and *In Vivo* Evaluation of Sol-Gel Derived TiO_2 Coatings Based on a Variety of Precursors and Synthesis Conditions

Krzysztof Marycz,[1,2] Justyna Krzak,[3] Wiktor Urbański,[1] and Celina Pezowicz[4]

[1] *Electron Microscope Laboratory, University of Environmental and Life Sciences Wroclaw, Ulica Kożuchowska 5B, 50-631 Wroclaw, Poland*
[2] *Wrocławskie Centrum Badań EIT+, Stablowicka 147 Street, 54-066 Wroclaw, Poland*
[3] *Institute of Materials Science and Applied Mechanics, Wroclaw University of Technology, Ulica Smoluchowskiego 25, 50-370 Wroclaw, Poland*
[4] *Division of Biomedical Engineering and Experimental Mechanics, Wroclaw University of Technology, Ulica Lukasiewicza 7/9, 50-371 Wroclaw, Poland*

Correspondence should be addressed to Krzysztof Marycz; krzysztofmarycz@interia.pl

Received 19 February 2014; Revised 17 April 2014; Accepted 5 May 2014; Published 1 June 2014

Academic Editor: Zhongkui Hong

The effect of synthesis way of TiO_2 coatings on biocompatibility of transplanted materials using an *in vitro* and *in vivo* rat model was investigated. TiO_2 layers were synthesized by a nonaqueous sol-gel dip-coating method on stainless steel 316L substrates applying two different precursors and their combination. Morphology and topography of newly formed biomaterials were determined as well as chemical composition and elemental distribution of a surface samples. *In vitro* tests were conducted by adipose-derived mesenchymal stem cells cultured on TiO_2 coatings and stainless steel without coatings to assess the bioreactivity of obtained materials. A positive biological effect of TiO_2/316L/1 coatings—based on titanium(IV) ethoxide—was found in both *in vitro* and *in vivo* models. The TiO_2/316L/1 exhibited the highest roughness and the lowest titanium concentration in TiO_2 than TiO_2/316L/2—based on titanium(IV) propoxide and TiO_2/316L/3—based on both above-mentioned precursors. The proper fibroblast-like morphology and higher proliferation rate of cells cultured on TiO_2/316L/1 were observed when compared to the other biomaterials. No inflammatory response in the bone surrounding implant covered by each of the obtained TiO_2 was present. Our results showed that improvement of routinely used stainless steel 316L with TiO_2/316L/1 layer can stimulate beneficial biological response.

1. Introduction

One of the most important factors in bone regeneration process is the biocompatibility of transplanted materials. It implies the proper response of the living tissue to materials implanted, expressed by the lack of allergic, toxic, and/or inflammatory reactions [1]. In the last two decades, much attention has been paid to thorough investigations of different metallic prostheses applied in the treatments of bone pathologies [2–4]. Among various metallic devices in the field of human orthopedics, stainless steel 316L (SS 316L) is still the most commonly used material. It is usually utilized as a material for short-term implant constructions such as wires, plates, or nails [5]. Despite its benefits such as (i) desirable biomechanical properties, (ii) ease of manufacturing, (iii) availability, and (iv) inexpensiveness, this alloy is also characterized by some disadvantages. The most significant are low resistance to corrosion in tissue environment and poor biocompatibility. SS 316L, exposed to the body fluids, releases highly toxic iron ions, which can cause abnormal proliferation and cell differentiation, and in consequence, can lead to the local inflammation, fibrosis, or even necrosis [6].

The solution to this problem is covering the austenitic steel with suitable coatings, which constitute a protection layer against the release of heavy ions that does not interfere

with the biomechanical properties of the substrate material. Moreover, advanced coating may (i) contain organic compounds with pharmacological properties, (ii) result a proper roughness or porosity at nano- or submicroscale, and also (iii) give a chemical composition, which allows for a permanent connection on the border tissue-implant. In order to improve the biocompatibility of routinely applied stainless steel materials, a broad range of coating techniques has been developed and applied [7–9]. One of the most frequently used methods in the field of bioengineering is the sol-gel dip-coating technique. It is often applied to the projections of commercial implants as well as to the sol-gel materials [10].

Constantly developing tissue engineering (TE) provides new chemicals, which may find wide applications in the design of effective and durable implants [8, 9]. One of the best described and investigated chemicals in orthopedic and oral implantology is titanium dioxide (TiO_2). Naturally forming active thin layer of TiO_2 on titanium alloy is known to be a factor enhancing osteoblast adhesion and inducing cell growth. Moreover, it is responsible for the biocompatibility of titanium alloys [11–13]. On the other hand, formation of natural TiO_2 layer *in vivo* is a lengthy process and occurs in random areas of the implant [10]. Additionally, due to the high costs of titanium implants, their availability for patients in medical practice is often limited.

Rapidly growing interest of many research groups around the world, concerning the development of new cell therapies using mesenchymal stem cells (MSCs), seems to be a promising direction for the future of regenerative medicine [14]. It was reported that MSCs isolated from adult tissue together with permanent and/or committed cells, that is, osteoblast and fibroblasts (routinely used in biomaterial testing), have unique capacity for self-renewal and plasticity [14–16]. Moreover, they possess the ability to differentiate into other cell types, for instance, osteoblasts, chondrocytes, or adipocytes [17]. These properties make MSCs a natural indicator of the biocompatibility of biomaterials, which from the clinical point of view might become a promising therapeutic tool. Moreover, stromal stem cells exhibit a higher cellular plasticity, and even slight chemical or structural changes in their environment may interfere with proper cellular adhesion and proliferation rate—features strongly correlated with the subsequent clinical outcomes [18]. Therefore, testing the biocompatibility of biomaterials by the application of MSCs appears to be the most effective and suitable way to evaluate the usefulness of novel coatings.

In the present study, various thin TiO_2 films were synthesized by a nonaqueous sol-gel dip-coating method on stainless steel 316L substrates, using different precursors and their combination. The morphology and topography of newly formed biomaterials were evaluated by means of scanning electron microscopy (SEM) and atomic force microscopy (AFM). Furthermore, the chemical composition and elemental distribution of the synthetic surface of coatings were determined by energy-dispersive X-ray spectroscopy (SEM-EDX) and Raman spectroscopy, respectively.

Application of different precursors as well as various synthesis conditions in the sol-gel process may affect the formation of the final product and, in consequence, result in biomaterials of different biological activity. Based on these facts, the influence of three distinct syntheses of TiO_2 coatings on the biocompatibility using *in vitro* and *in vivo* rat models was investigated. In the first part of the study, the bioreactivity of biomaterials tested *in vitro* using adipose derived mesenchymal stem cells (AdMSCs) was evaluated. Detailed analysis of AdMSCs cultured on specific surfaces comprising cell morphology, cytotoxicity assay, and proliferation factor allowed to select most bioactive layers for testing in an *in vivo* model. The results of experiments conducted revealed that titanium dioxide synthesized in a different manner can lead to the formation of biomaterials of different reactivity, which in turn can affect the quality of further treatment.

2. Materials and Methods

2.1. Substrate Preparation. Metal substrates for *in vitro* tests were austenitic steel 316L (Inox Sp.j.) discs 15 mm in diameter and 1 mm thick. The metallic substrates in terms of mechanical properties, chemical composition, grain size, and the degree of contamination of nonmetallic inclusions meet the requirements of standards PN-ISO 5832-1:1997/A1:1999.

The samples were washed in a commercial detergent/water cleaning system and sonicated in acetone. Then, they were washed in water and ethanol. Next, the discs were dried at room temperature. For *in vivo* experiments, 10 mm long rectangular implants, with a 1×1 mm square base, were coated. Materials intended for implantations were sterilized in 150°C before transplantation.

2.2. Synthesis of TiO_2 Coatings. The surfaces of clean samples were coated with three various types of sol-gel hydrolysates by dip-coating method. In order to obtain three-layer coatings, each hydrolysate was applied three times. The hydrolysates were prepared using titanium(IV) ethoxide (TIEO; Sigma Aldrich), titanium(IV) propoxide (TIPO; Sigma Aldrich) as well as iso-propanol (iPrOH; POCH SA), and acetylacetone (AcAc; Sigma Aldrich) in the following volume ratio:

(1) TiO_2/316L/1—TIEO : iPrOH : AcAc (3 : 9 : 3);

(2) TiO_2/316L/2—TIPO : iPrOH : AcAc (3 : 9 : 3);

(3) TiO_2/316L/3—TIEO : TIPO : iPrOH : AcAc (1.5 : 1.5 : 9 : 3).

Substrates with a proper volume ratio were mechanically stirred for two hours at a speed of 250 rpm; then sols were aged for 24 hours. Afterwards, the discs were dip-coated in hydrolysates with a controlled parameters; the speed of dipping and pulling was set on 34 mm/min. The residence time of the substrate in the hydrolysate depended on the amount of layers deposited on the discs (1st layer—60 s, 2nd layer—30 s, and 3rd layer—15 s). This procedure of the sol-gel synthesis was conducted without water addition. Water needed for hydrolysis was derived in the form of moisture from the atmosphere, according to the method described previously [19, 20].

2.3. Surface Morphology. In order to investigate the surface morphology and topography of obtained biomaterials, SEM (Evo LS 15 Zeiss) and AFM (XE-100 Park Systems) were used. The discs were attached to SEM table and coated with gold in 300 seconds using a Gold sputter (Oxford 1-MS). The evaluation of biomaterials morphology was determined by Bruker SE detector SE at 500x magnification. AFM images were obtained using contact mode. The force constant of the tip NCS36/Al BS from MikroMasch was approximately 1 N/m and the resonance frequency was around 90 kHz. The area of investigated discs was $45 \times 45\,\mu$m. Roughness and texture of coatings were described as follows: R_a is arithmetic average roughness; R_q is root mean square roughness. The analysis was conducted according to ISO 4287 standards. The roughness of the surface was calculated based on the standard formula integrated in the software.

2.4. Chemical Composition and Elemental Distribution of Coatings. The chemical structure of obtained coatings was analyzed using Raman spectroscopy (LabRAM HR800 Horiba Jobin Yvon). The incident laser excitation was provided by a water-cooled argon laser source operating at 514.5 nm. Spectra were recorded in the $4000 \div 50\,\text{cm}^{-1}$ region with a spectral resolution of $2.5\,\text{cm}^{-1}$. The quantification analysis and the distribution of elements on the surface of biomaterials tested were determine using SEM energy-dispersive X-ray spectroscopy (EVO LS 15, EDX), according to the protocol described previously [21].

2.5. Ethical Approval. The experiment was approved by the Second Local Ethic Commission, Wroclaw, Poland; decision number 86/09: 84/2012.

2.6. Isolation and Propagation of AdMSCs. Adipose-derived mesenchymal stem cells (AdMSCs) were isolated from subcutaneous fat tissue of adult Wistar rats using technique described previously [22, 23]. Cells were maintained at 37°C in a humidified atmosphere of 5% CO_2 and 95% air. Primary cultures were propagated in Dulbecco's Modified Eagle's Medium (DMEM) and Nutrient F-12 Ham, whereas subsequent cultures were maintained in DMEM with high glucose (4500 mg/L). Media were supplemented with 10% of FBS and 1% of antibiotics and changed every two days. The passage of cells was performed when they reach 80–90% confluence. Before the test, cultures were passaged three times using trypsin (TrypLE; Life Technologies) according to the manufacturers' instruction.

2.7. Cytotoxicity of Biomaterials and Cell Proliferation Rate. Cytotoxic effect of materials synthesized to AdMSCs was evaluated using Alamar Blue assay (Sigma Aldrich) according to the instructions supplied. For the test, cells were seeded at a concentration of 35×10^3 in 24-well culture plates coated with the biomaterials obtained. The experiment was carried out in duplicate. Cell proliferation ratio was evaluated after 24, 48, 120, and 168 hours after inoculation. To determine the effect of coatings formed on the proliferative activity of cells, the cultures on uncoated SS 316L steel were carried out simultaneously and served as test controls. Normalization of the data with respect to the control cultures as well as the determination of the proliferation factor (PF) allowed us to identify biomaterials where modification of the surface resulted in an increase (PF > 1) or a decrease (PF < 1) of cell proliferation rates.

2.8. Calculation of Population Doubling Time. Analysis of population doubling time was performed using formula described earlier [24]. The number of cells was calculated using the growth curve determined in parallel with the cytotoxicity test.

2.9. Evaluation of AdMSCs Growth Pattern and Nuclei Visualisation. Morphology of cells and growth pattern were evaluated under inverted fluorescent microscope (Axio Observer.A1, Zeiss). All procedures were performed according to the manufacture's procedures, as described previously [25]. Prior to staining, cells were fixed in 4% ice cold paraformaldehyde for 10 minutes at room temperature. Afterwards, cells were washed three times in Hank's Balanced Salt Solution (HBSS, Sigma Aldrich, washing buffer containing 1% of fetal bovine serum), permeabilized with 0.1% Triton X-100, and washed again with the buffer (three times before staining) at room temperature. Then, cells were stained with 4′,6-diamidino-2-phenylindole (DAPI; Sigma Aldrich) using 5 μg of dye per 1 mL of HBSS. After staining, preparations were thoroughly washed and evaluated under the epifluorescence microscope. Images were captured with Power Shot Camera A630 8 MP (Cannon).

2.10. Animals and Surgery. Sixteen male Wister rats, aged between 3 and 6 months and weighing over 300 g, were used in the experiment. Animals were randomized and divided into two groups: a control group (uncoated SS 316L implants; $n = 8$) and experimental group (implants coated with TiO_2; $n = 8$). All animals were kept in the same room in standard conditions (12 h : 12 h of light-dark cycle, room temperature 20.5°C ± 1°C) in separate cages with free access to water and feed, without movement restrictions. Surgical procedures were performed in general anaesthesia in aseptic conditions. In order to anaesthetize the animals, 1 mL of ketamine hydrochloride (100 mg/mL) and 0.5 mL of xylazine hydrochloride (20 mg/mL) was injected intraperitoneally in a dose of 1 mL/100 mg of body weight. Subsequently, the left leg was shaved and washed in a chlorhexidine solution positioned on the operating table and clothed in sterile sheets. On the lateroanterior knee surface, 10–15 mm curved incision was made. Lateral to the knee patella, articular capsule and patella were subluxated to expose a femur intercondylar fossa. The medullar canal of the femur was opened through intercondylar fossa with a drill of 1.2 mm in diameter. Next, the implants were positioned in the medullar canal and the wound was closed. Animals were sacrificed after twelve weeks from implantation by injection of sodium pentobarbital (Morbital) in a dose of 2 mL/kg of body weight. The part of left femur with an implant was dissected and clinically evaluate.

2.11. Tissue Samples Preparation. After the experimental period, the bone with implants was removed and fixed in 10%

buffered formalin and embedded in paraffin. Parts of the bone with an implant were used in SEM analysis, whereas other sections were applied for histological investigation (Zeiss Microm HM 340E).

2.12. Hematoxylin and Eosin Staining. Bone samples were fixed in 10% buffered formalin and embedded in paraffin. After tissue processing and paraffin embedding, 5 μm thick sections were stained with haematoxylin and eosin (Shandon). Tissues surrounding the implants were viewed and evaluated using light microscope (Carl Zeiss Axio Imager A1).

2.13. Immunohistochemistry. Bones were cut with a microtone (Zeiss Microm HM 340E) into 3 μm thick sections and placed on histological slides. Next, the specimens were deparaffinized and hydrated in xylene and alcohol graded series. After the fixation and dehydration steps, specimens were incubated in Tris/EDTA buffer (pH = 9.0) for 20 minutes to carry out a heat-induced epitope retrieval. Endogenous peroxidise activity was blocked in 3% hydrogen peroxide for 5 minutes, and then the samples were briefly rinsed with TBS (3 × 5 minutes). Tissue samples were incubated for 1 hour at room temperature with primary antisera raised against the IL6, (Rat, working dilution 1 : 400; Abcam), TNF Receptor I (Rat, working dilution 1 : 1000; Abcam), and Caspase-1 (Rat, working dilution 1 : 5; Abcam). After subsequent rinsing in TBS (3 × 5 minutes), the sections were incubated with secondary antibodies (working dilution; EnVision Systems; Dako) for 1 hour at room temperature. Subsequently, samples were counterstained with Mayer's haematoxylin, dehydrated in alcohol and xylene series, then mounted with permanent mounting medium, and finally covered with a glass coverslip. High resolution images were captured under light microscope (Carl Zeiss Axio Imager A1) at 40x magnification. Then, images were processed (same parameters were applied to all images) and histomorphometry was performed. AxioVision Rel. 4.6.3 (Carl Zeiss) software was used to identify the cells containing cytokines tested as well as estimate the total area for comparison between groups.

2.14. Statistical Analysis. Statistical analysis of independent and dependent variables, with respect to the total area (μm^2) of tissue containing cytokines, was performed using two-way analysis of variance (ANOVA). Based on the results obtained from ANOVA, t-test was applied to compare individual differences between the means for stainless steel 316L implants coated with TiO_2 and uncoated implants as a control group. The differences with a probability of $P \geq 0.05$ were considered significant. Mann-Whitney U test or Wilcoxon test were applied for nonparametric analysis. To verify whether the t-test can be used, normal distribution of the variables was checked with Shapiro-Wilk test and homogeneity of variance with Brown and Forsythe test.

Table 1: Characteristics of the surface roughness parameters for the particular titania dioxide coatings as measured by AFM.

Substrate	Layer	R_a (nm)	R_q (nm)
Stainless steel 316L	Pure	164	255
	TiO_2/1	210	280
	TiO_2/2	190	230
	TiO_2/3	150	190

R_a: arithmetic average roughness; R_q: root mean square roughness.

3. Results

3.1. Physicochemical Investigation of Biomaterials

3.1.1. Surface Morphology and Topography. The morphology of uncoated SS 316L and its surface modifications are presented in Figure 1. The morphology of stainless steel 316L substrate had clear grain boundary (Figure 1(a)), while the titania dioxide coatings were smooth, transparent, and homogenous (Figures 1(c), 1(e), and 1(g)). The titania dioxide layers tested covered stainless steel 316L in a uniform manner. Atomic force microscope (AFM) analysis revealed differences in the submicroroughness of the surface of particular titania dioxide coatings (Figures 1(d), 1(f), and 1(h); Table 1). TiO_2/316L/1 layer exhibited highest arithmetic average roughness equal to R_a = 210 nm, while TiO_2/316L/3 had lowest R_a index (150 nm), which was slightly lower than the R_a of 316L (160 nm). Intermediate average of submicroroughness of the surface was recorded for TiO_2/316L/2 coatings (R_a = 150 nm).

3.1.2. SEM-EDX and Raman Spectroscopy. Combined SEM-EDX and Raman spectroscopy analysis allowed evaluating both the elemental composition and distribution on the coating as well as the physicochemical structure of layers (Figure 2). SEM-EDX analysis revealed uniform distribution of titanium on the surface of biomaterials synthesized (Figures 2(b), 2(d), and 2(f)). Micro X-ray analysis demonstrated the lowest titanium concentration in TiO_2/316L/1 layer, which was equal to 19.18 (wt.%). In TiO_2/316L/2 and TiO_2/316L/3, a higher content of titanium was detected, 21.80 (wt.%) and 31.61 (wt.%), respectively (Table 2).

The Raman spectrum of SS316L, as a substrate for layer, was presented in Figure 2(a). The range of spectrum has been adapted to the TiO_2 spectra. This is explained below. The bands on SS316L spectrum have a relatively low intensity. The characteristic bands of SS316L disappeared on the TiO_2 spectra what can indicate their covering by the bands characteristic for TiO_2.

Raman spectra of TiO_2 coatings, annealed at 250°C, on metallic substrate (SS316L) were shown in the range 900–50 cm^{-1} due to the presence of all modes characteristic for the anatase phase (Figures 2(c), 2(e), and 2(g)). Analysis of the fundamental vibrations of anatase, crystalline form of titanium dioxide, shows that six vibrations active in Raman spectra can be expected: A1g + 2B1g + 3Eg. These vibrations bands are observed in the TiO_2 coatings spectra as follows:

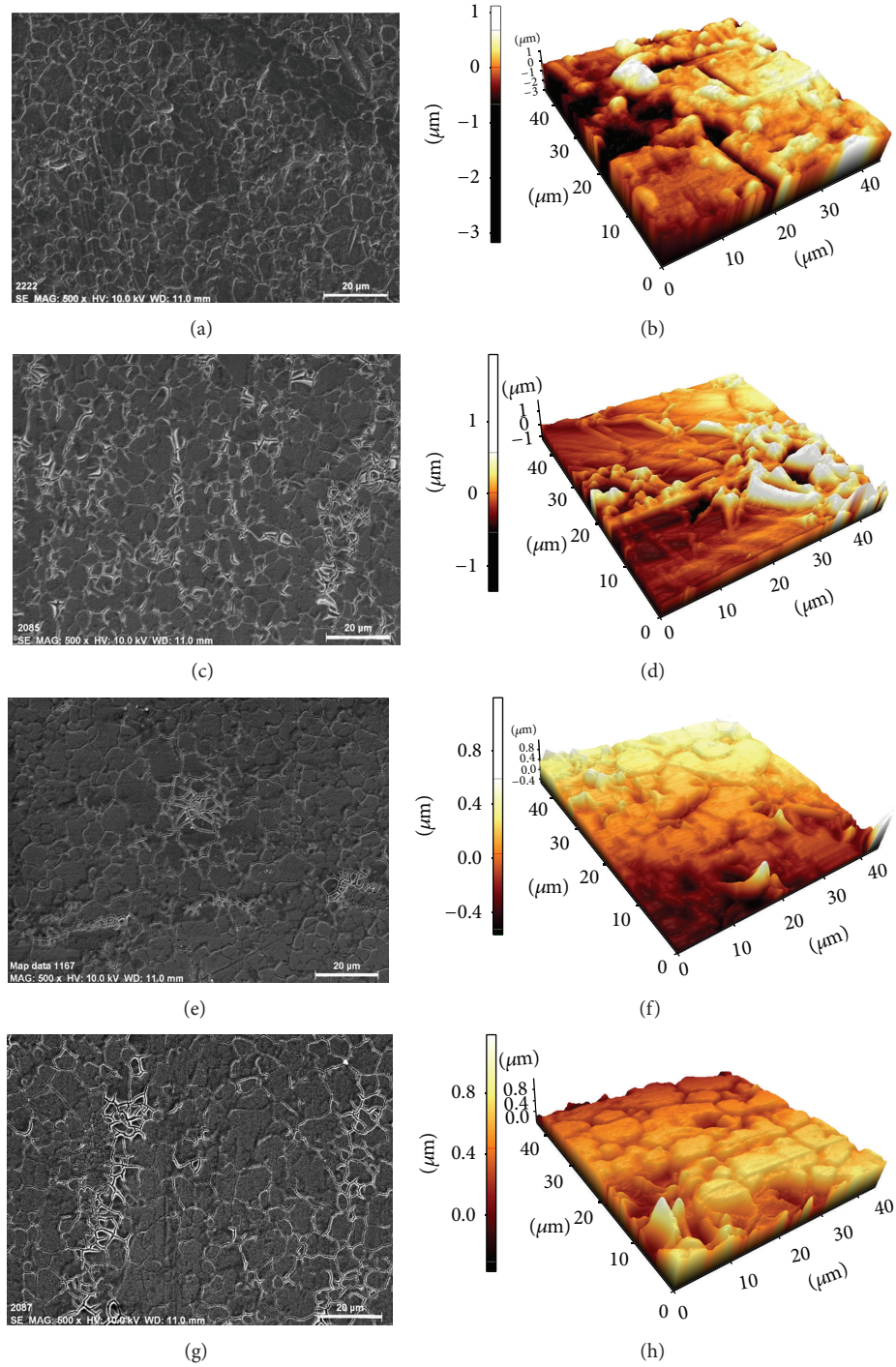

FIGURE 1: Scanning electron microscope (SEM) images ((a), (c), (e), and (g)) at 500x magnification and atomic force microscope (AFM) surface morphology images ((b), (d), (f), and (h)) of TiO_2/316L/1 ((c), (d)), TiO_2/316L/2 ((e), (f)), and TiO_2/316L/3 ((g), (h)) layers deposited on stainless steel 316L ((a), (b)).

peaks marked, at each spectrum shown in Figures 2(c), 2(e), and 2(g), as "A": at about 150, 205, and 605 cm^{-1} correspond to Eg modes. The peaks at 390 cm^{-1} marked as "B" correspond to B1g mode and the peak marked as "C" at 515 cm^{-1} correspond to A1g anatase modes.

3.2. The Morphology, Proliferation Rate, and Population Doubling Time of AdMSCs Cultured on TiO_2 Layers and Stainless Steel. Adipose derived mesenchymal stem cells (AdMSCs) seeded on TiO_2/316L/1 coating exhibited fibroblast like morphology with pronounced di-, three-, and multipolar shape,

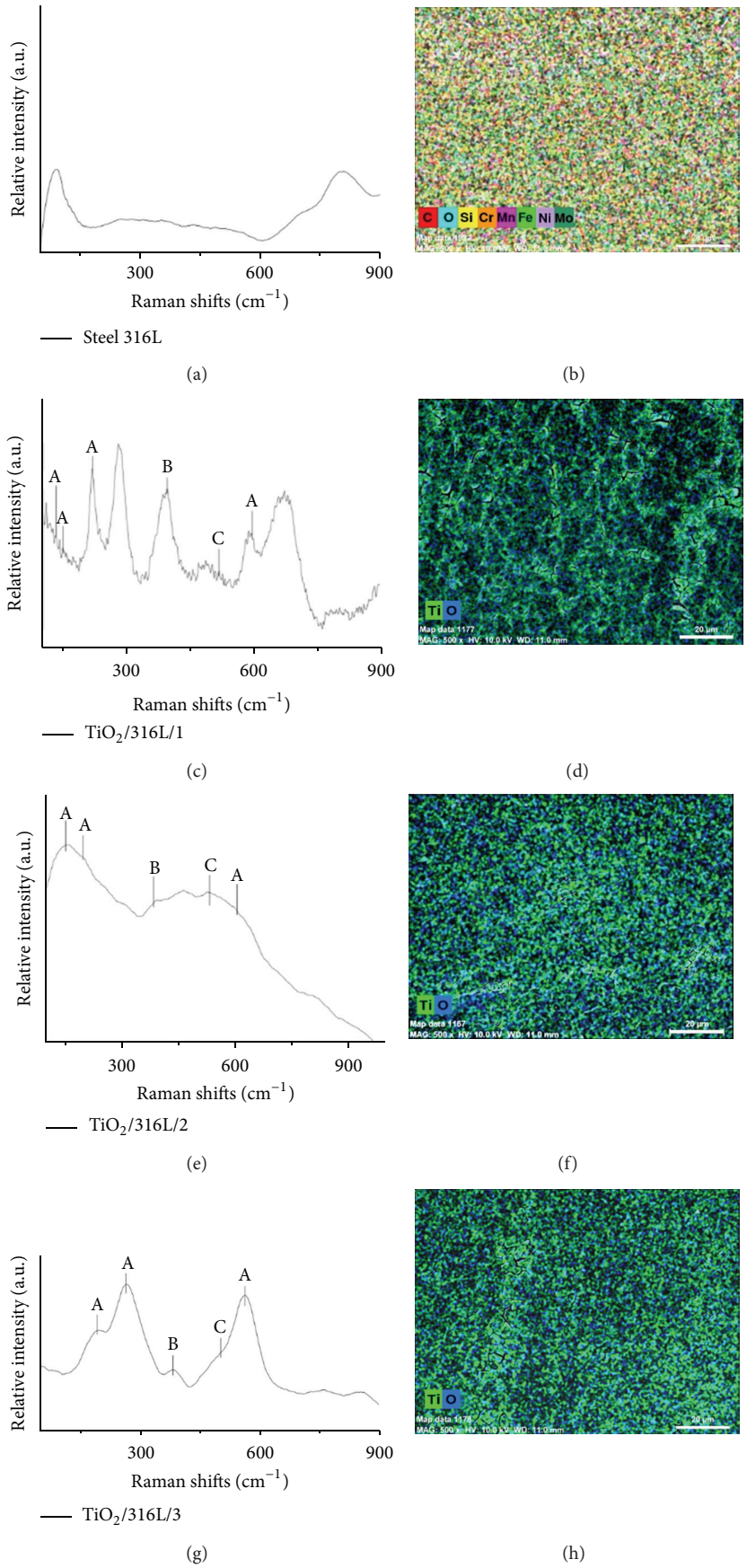

Figure 2: Raman spectra and SEM-EDX mapping images of elements' distribution in pure stainless steel ((a), (b)) and titania dioxide coatings ((c), (d), (e), (f), (g), and (h)). The bands were marked by (A, B, C) at the spectra.

Table 2: Quantitative analysis of SEM-EDX and SEM-EDX spectra of stainless steel (SS 316L) and the sol-gel synthesis of titania-derived coatings: TiO_2/316L/1, TiO_2/316L/2, and TiO_2/316L/3.

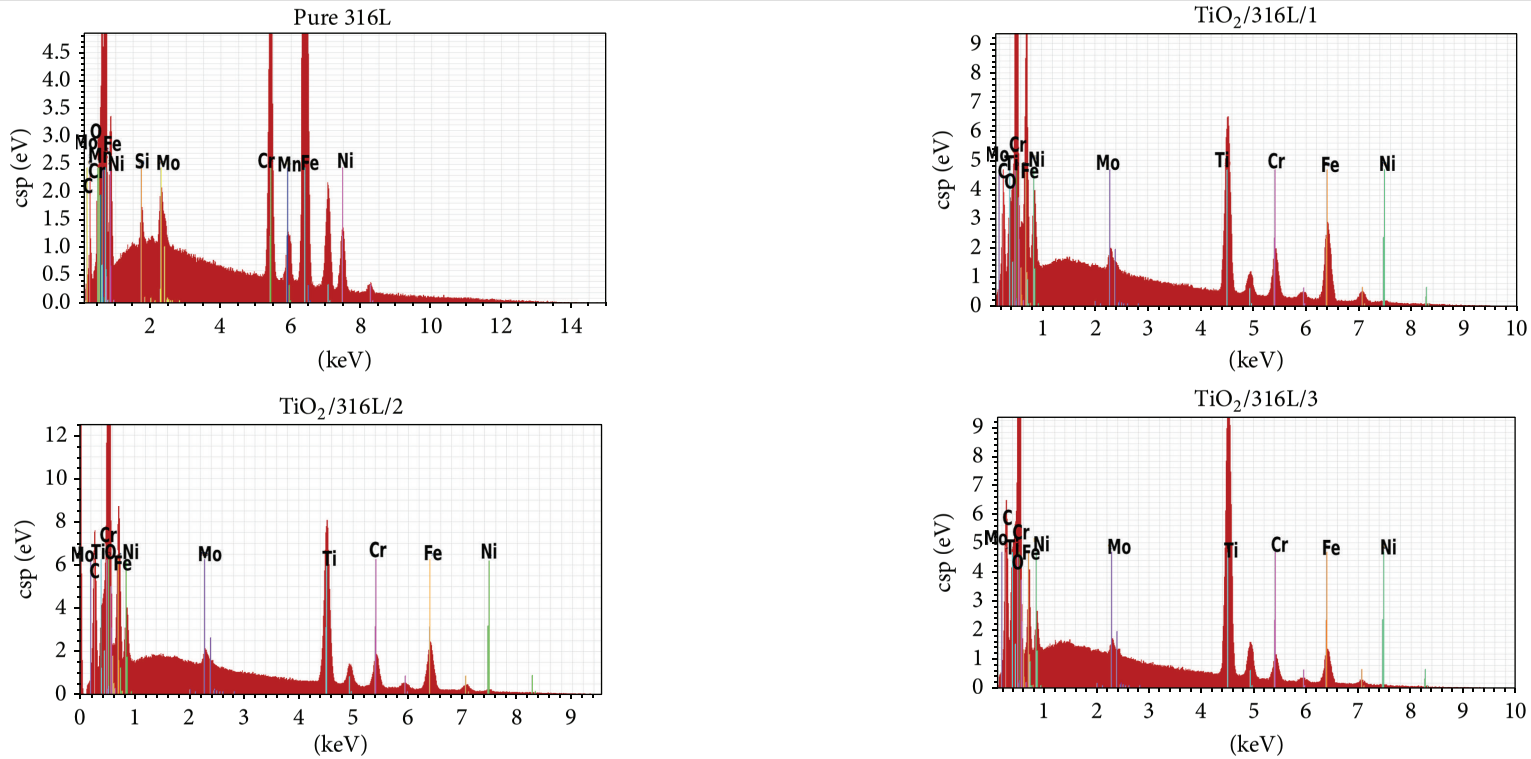

Element	Pure 316L		TiO_2/316L/1		TiO_2/316L/2		TiO_2/316L/3	
	wt [%]	error	wt [%]	error	wt [%]	error	wt [%]	error
C	0.78	±0.1	1.83	±0.3	3.57	±0.5	3.33	±0.4
O	0.39	±0.1	12.13	±6.5	16.12	±7.6	20.82	±9.7
Ti	0.0	±0.0	19.18	±0.7	21.80	±0.8	31.61	±1.1
Cr	15.12	±0.5	10.11	±0.4	8.51	±0.3	5.71	±0.2
Fe	67.83	±2.0	39.02	±1.7	29.74	±1.3	19.16	±0.9
Ni	10.00	±0.3	8.30	±1.1	7.21	±1.0	4.48	±0.7
Mo	3.48	±0.1	1.28	±0.1	1.11	±0.1	0.90	±0.1

Table 3: The values of the proliferation factor (PF) obtained for AdMSCs cultures in the context of the applied surface.

Substrate	Layer	Duration of the cell culture [h]			
		24	48	72	168
Stainless steel 316L	Pure	1	1	1	1
	TiO_2/1	0.92	0.80	0.85	1.48
	TiO_2/2	1.00	0.90	0.93	0.93
	TiO_2/3	0.80	1.32	1.00	1.02

Table 4: Statistical analysis ($n = 10$) of cytokine levels around stainless steel 316L and titania dioxide (TiO_2) coated implants.

Cytokine	Mean SS 316L	Mean SS 316L + TiO_2	P value
IL-6	50115	10241	6.59×10^{-5}
Caspase-1	50561	11550	3.13×10^{-6}
TNF-alpha	36463	12683	10.56×10^{-5}

during 168-hour culture (Figures 3(c) and 3(d)). In comparison to control culture, TiO_2/316L/1 coating stimulated AdMSCs to form fully developed cellular monolayer with a dense network of intercellular connections. Morphological analysis of AdMSCs seeded on TiO_2/316L/2 (Figures 3(e) and 3(f)) and TiO_2/316L/3 (Figures 3(g) and 3(h)) revealed focal stem cell distribution with increasing frequency AdMSCs cultured on pure stainless steel formed aggregates and displayed signs of degeneration by apoptosis.

Stem cells seeded on TiO_2/316L/1 and TiO_2/316L/2 were comparable in size, as opposed to control (Figures 3(a) and 3(b)). TiO_2/316L/3 coating caused the development of AdMSCs differing in size with a tendency to extreme aggregations in specific areas of the material. Additionally, the presence of large amounts of cytoplasm and spontaneously occurring giant cells was observed in TiO_2/316L/3 (Figures 3(g) and 3(h)) and control cultures (Figures 3(a) and 3(b)). Centrally located nuclei were found in AdMSCs cultured on TiO_2/316L/1, while in TiO_2/316L/2 and TiO_2/316L/3 nuclei were peripheral. Moreover, DAPI staining allowed estimating to some extent the spatial distribution of investigated cultures because of the nonspecific labelling of the cytoplasm. The highest density of cells was observed in TiO_2/316L/1 layer (Figures 3(c) and 3(d)) when compared with stainless steel (Figures 3(a) and 3(b)) and other TiO_2 coatings (Figures 3(e), 3(f), 3(g), and 3(h)). All cultures with the study biomaterials showed no signs of apoptosis and/or necrosis.

Proliferation ratio (PF) of AdMSCs cultured on TiO_2/316L/1 was substantially higher than on other titanium based biomaterials or stainless steel after 168 h culture. Interestingly, all of the investigated coatings reached higher PF after 168 h of culture compared to stainless steel-based material. Results of the calculations of proliferation ratios are presented in arbitrary units (Table 3). Analysis of proliferation ratio confirmed that the modification of metallic substrate with TiO_2/316L/1 coating stimulated the proliferation of AdMSCs most effectively.

When population doubling time (PDT) is considered, TiO_2/316L/1 coatings resulted in the lowest PDT than TiO_2/316L/2 and TiO_2/316L/3 layers as well as control. In case of TiO_2/316L/2 coatings the highest PDT was observed as compared to the other titania layers and stainless steel (Figure 6).

3.3. Postmortem Macroscopic Evaluation. Surgical exposure sites healed properly in all animals with no signs of infection. Entry points to marrow canals were covered by fibrous cartilage and knee articulations were normal. In the control group (uncoated stainless steel 316L implants), new bone formation was not observed. Implants were mobile and covered spontaneously with white fibrous-like tissue. Cortical bone was thin, irregular, and in some locations exhibited osteolytic character. Macroscopic evaluation of the titania dioxide implants revealed strong mechanical fixation in all experimental animals. New bone formation was observed around the implanted materials and no symptoms of inflammatory or fibrous tissue were observed.

3.4. Haematoxylin and Eosin (H&E), Immunohistochemistry, and SEM Evaluation. Histological evaluation of the control materials, consisting of eight samples ($n = 8$), revealed in the majority of estimated pictures inflammation of the bone surrounding the implant. The abundant granulation of the tissue, lymphocyte, and granulocyte infiltration in seven from eight individuals was observed (Figures 4(a), 4(b), and 4(c)). Significant higher level of TNF-alpha (Figure 5(a)), IL-6 (Figure 5(b)), and Caspase-1 (Figure 5(c)) was recorded in comparison to the titania dioxide implant (Table 4). Rich fibrous tissue was observed around the implanted stainless steel material as well as symptomatically formed bone. SEM analysis revealed only local bone attachment to the austenitic steel implant (Figure 4(d)) in seven out of eight individuals studied. The inflammatory response was decreased in the group where titania dioxide surface was applied (Figure 4(e)). Experimental implant covered by titania dioxide did not cause inflammatory reaction of the bone surrounding the implant in any of the subjects assessed ($n = 8$) (Figures 4(f) and 4(g)). Although no fibrous tissue was observed directly adhering to the material and fibroblasts, extensive bone formation with slight degree of osteolysis and granulocyte infiltration was noticed in one individual (Figure 4(g)). SEM technique showed a significant bone attachment to the titania dioxide biomaterials in eight individuals evaluated ($n = 8$) (Figure 4(h)).

4. Discussion

Nowadays, increasing attention is paid to the development of metallic materials for orthopedic applications. This is due to the large demand of contemporary society, resulting from the development of various diseases of civilization. According to Schneider et al. [26] more than one million of bone grafts and orthopedic interventions are needed worldwide every year. These statistics emphasize the increasing demand for metallic devices, which are an essential instrument in orthopedics.

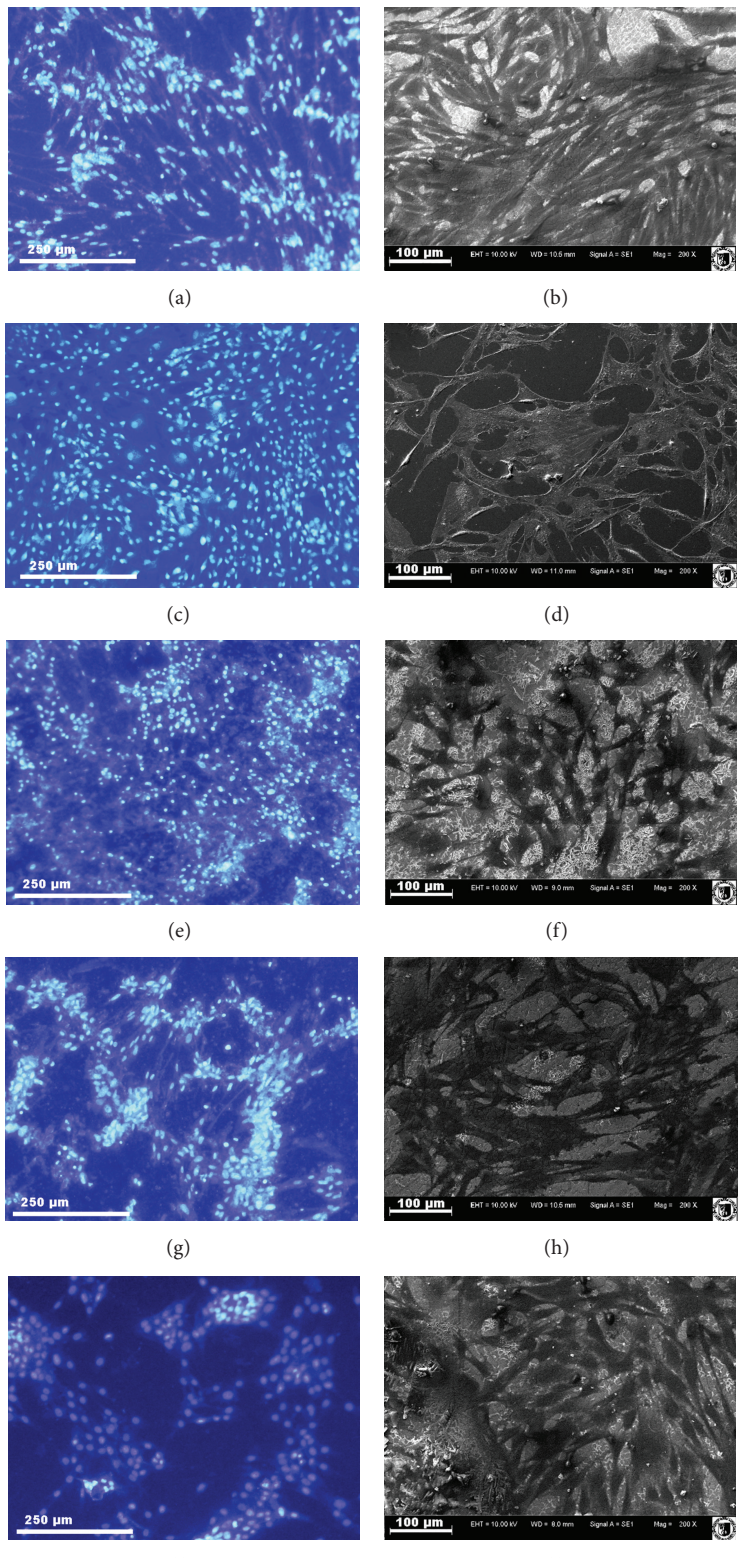

FIGURE 3: Morphology and growth pattern of AdMSCs cultured on stainless steel 316L ((a), (b)), glass coverslip ((c), (d)), TiO_2/316L/1 ((e), (f)), TiO_2/316L/2 ((g), (h)), and TiO_2/316L/3 ((i), (j)) coatings after 168 h of cell culture. Cells were stained with DAPI (nuclei are visible in light-blue), mag. 50x, scale bar: 250 μm (left). SEM images indicate the morphology of AdMSCs at 200x mag (right).

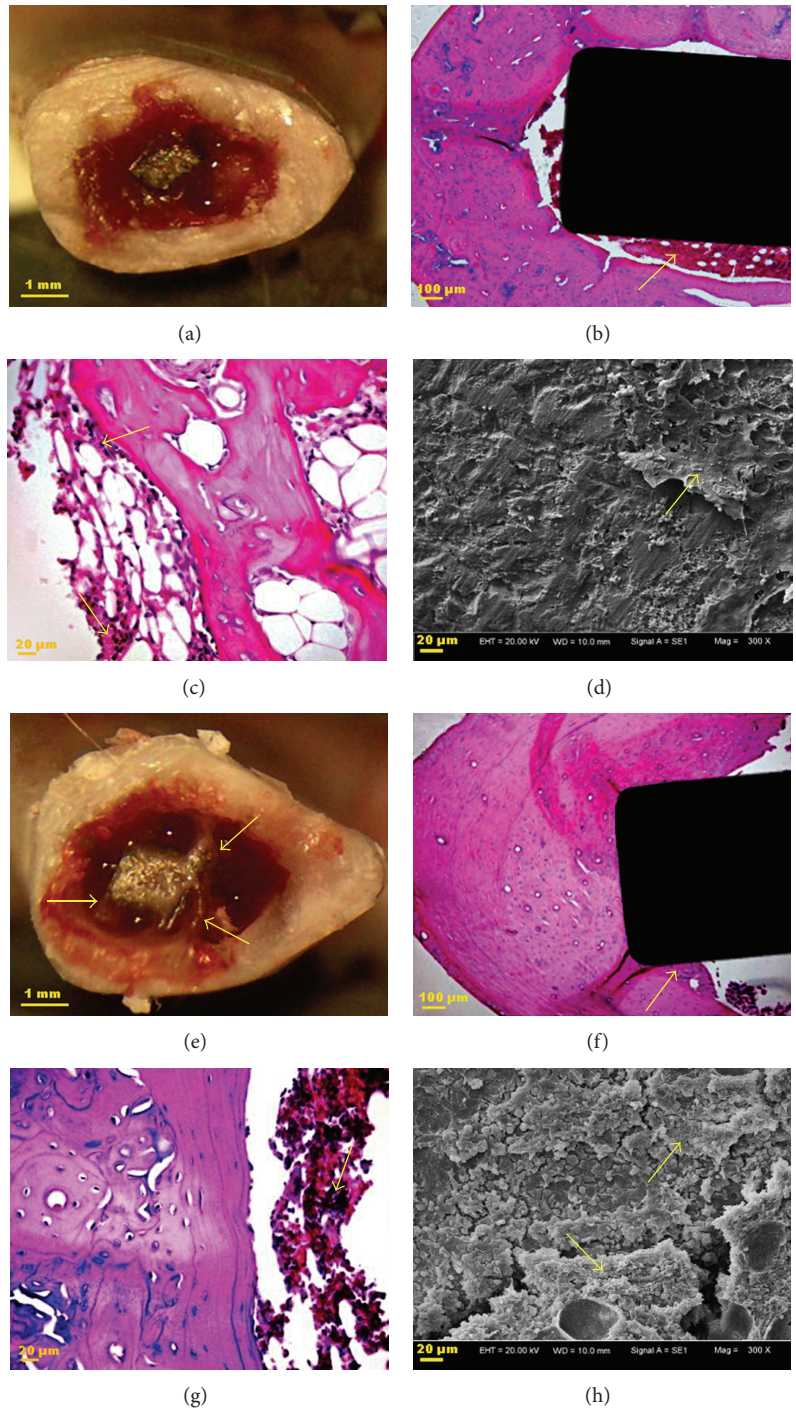

(a) (b)

(c) (d)

(e) (f)

(g) (h)

Figure 4: Hematoxylin and eosin-stained specimens ((a), (c), (f), and (g)) and SEM microphotographs ((d), (h)) illustrating the stainless steel (a) and titanium (e) implantsurrounded by the bone tissue. Inflammatory and fibroblastic response around the implanted stainless steel material characterized by leukocyte and macrophages infiltration ((b), (c); arrow). SEM picture revealed only the local bone attachment to the austenitic steel implant ((d); arrow). In the group where titania dioxide material was applied a decrease in the inflammatory response within the tissue surrounding the implant was detected ((f), (g); arrow). Extensive bone formation ((e); arrow) with slight degree of osteolysis and granulocyte infiltration ((g), arrow) was noticed. SEM technique indicated a significant bone attachment to the titania dioxide biomaterial ((h), arrow). Mag. 300, 1000x for control and experimental materials, respectively; scale bar: 200 μm.

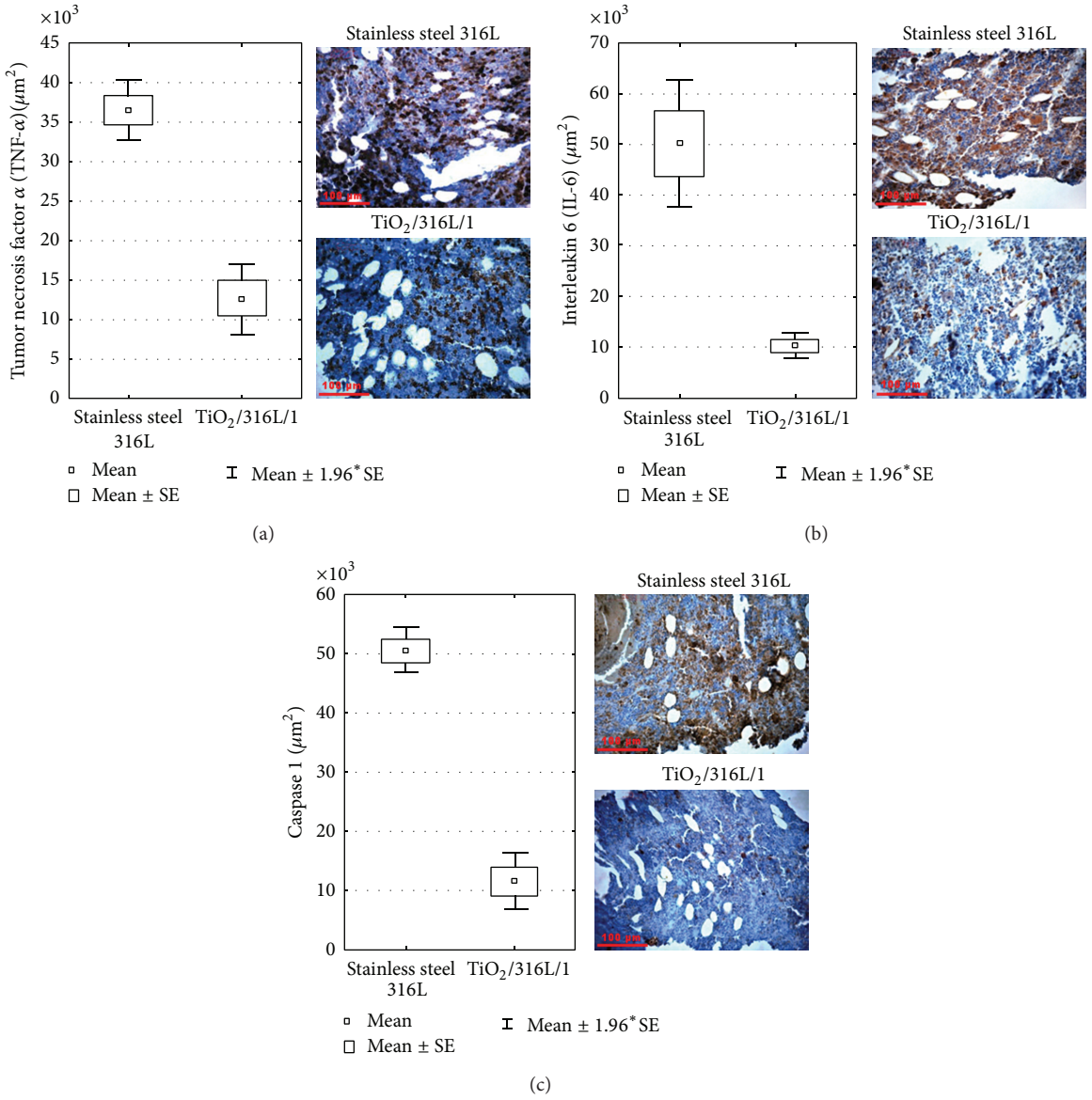

FIGURE 5: Cell area (μm^2) containing TNF-alpha (a), IL-6 (b), and Caspase-1 (c) signals and the mean values with standard deviations for each group. On the right side, images from the light microscope; specimen stained immunohistochemically (mag. 8 × 40) for TNF-alpha (a), IL-6 (b), and Caspase-1 (c). Dark stained cells contain high concentrations of TNF-alpha (a), IL-6 (b), and Caspase-1 (c).

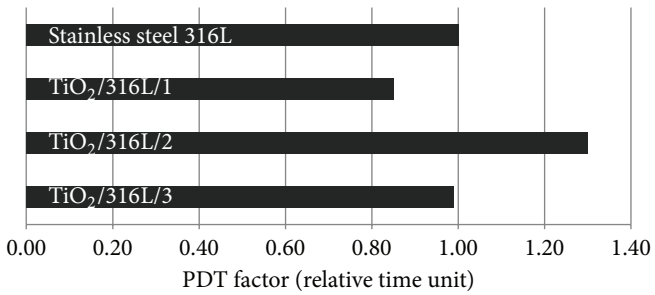

FIGURE 6: Calculation of the population doubling time. Values obtained for AdMSCs in the context of the applied surface.

Answer to this problem is the design of innovative materials with proper mechanical features and defined physicochemical structure, that is, high osteoinductive properties and proper bone integration that would decrease inflammation level in the surrounding tissue. Metallic materials have reasonably adequate mechanical properties. Furthermore, certain coatings of metallic substrates have been proved to be chemically stable and durable [27–30]. In the present study we investigated the biological effect of three differently synthesized thin TiO_2 layers, using various precursors, and coated on routinely applied stainless steel 316L substrate with known mechanical characteristics using the dip-coating method. The obtained biomaterials varied in morphology and topography as shown by AFM and SEM analyses. Our data demonstrated the highest roughness of TiO_2/316L/1 coating compared to TiO_2/316L/2 and TiO_2/316L/2 layers. The differences in the surface topography of biomaterials obtained might result from various synthesis conditions.

The presence of ethoxyl group from titanium(IV) ethoxide in case of TiO_2/316L/1, occurred during the incomplete hydrolysis, could be a reason of the creation of a shorter chains network TiO_2, what in consequence increases the surface roughness. In case of using the titanium(IV) propoxide (TiO_2/316L/2) as the precursors in the titania network the propoxyl group could stay after the incomplete hydrolysis and then the chains network are longer so the surface is smoother and homogenous in shape. Taking into consideration the incomplete hydrolysis in each case, it should be added that all achieved data, both physicochemical and biological, are repeatable. To synthesis of TiO_2/316L/3 both the abovementioned precursors were used, and the results are unsatisfactory. In addition, the lowest concentration of titanium in TiO_2/316L/1 coatings as well as formation of chemically stable Ti-O-Ti network was confirmed in physicochemical analyses. These parameters of biomaterials can substantially affect surface topography of the coatings. This data partially correlates with the earlier study [30], in which a positive biological influence of the titanium surface roughness on the proliferation of bone marrow mesenchymal stem cells was observed.

The three various titania dioxide layers were subjected to a cellular *in vitro* analysis using mesenchymal stromal stem cells of adipose origin (AdMSCs). Mesenchymal stem cells are multipotent; thus they can differentiate into other cells types, for example, osteoblasts [17]. In contrast to already committed cells, MSCs exhibit high phenotypic plasticity, which makes them unquestionable indicator of potential biomaterials [14–16]. In order to investigate cellular response to biomaterials tested, we developed a protocol that allowed us to identify the biomaterial of the highest biofunctionality. Among all TiO_2-based coatings tested, AdMSCs cultures on TiO_2/316L/1 had the highest value of the proliferation factor (PF), when compared to other titanium(IV) oxide biomaterials as well as the control culture. Furthermore, population doubling time factor (PDT) of tested materials indicated the lowest PDT in TiO_2/316L/1 coating when compared to other titanium(IV) oxide biomaterials and the control culture. It should be noted that other titania dioxide biomaterials also stimulated AdMSCs' proliferation, although these cells did not grow in a stable manner. What is more, AdMSCs formed fully developed monolayer extended on the surface of the test TiO_2/316L/1 coating in contrast to the control austenitic steel culture where the focal growth of mesenchymal stem cells was observed. This could be due to the application of TIEO precursor in the synthesis of TiO_2/316L/1 coating, which additionally stimulated AdMSCs towards formation of dense intercellular connections. It is worth noting that the application of TIPO and TIEO/TIPO mixtures in other titania based coatings had negative influence on AdMSCs, resulting in an unequal growth. It should also be stressed that AdMSCs colonized TiO_2/316L/1 in a uniform manner, suggesting their future osseointegrative effect on the *in vivo* model. Based on the AdMSC response introduced to TiO_2/316L/1 microenvironment, we decided to use this material for further *in vivo* experiments in a rat model.

Postmortem evaluation of the bone integration of biomaterials using a surgical microscope and microsurgical instruments revealed the development of newly formed bone around the TiO_2/316L/1 implant. Histological examination confirmed these observations and additionally showed the lack of fibrosis and/or necrosis formation in the tissue surrounding the implant, as opposed to stainless steel materials. What is more, slight macrophage infiltrations in TiO_2/316L/1 implant were observed, while in the case of stainless steel, numerous macrophages were observed. Scanning electron microscopy analysis confirmed the significant development of callus on the surface of the TiO_2/316L/1 material, which also indicated a satisfactory implant osseointegration. In case of the implant made from uncoated SS 316L, only spherical development of new bone was observed.

Proinflammatory cytokines such as IL-6, TNF-alfa, and Caspase-1, in addition to their important role in inflammation process, are crucial indicators of the bone osteolysis process [20, 21, 31]. High concentrations of these proteins were reported in the tissues surrounding loose endoprostheses [31, 32]. Our study showed lower concentration of IL-6, TNF-alfa, and Caspase-1 in tissues with titania based materials compared to the tissue with stainless steel. The reduced concentration of these proinflammatory cytokines may improve implant-bone bonding and create implants more resistant to aseptic loosening. Anti-inflammatory properties of TiO_2 based biomaterials may be connected with their antioxidant properties. According to the study of Contreras et al. [33] titanium oxide significantly reduces the level of reactive oxygen (free radicals), thus decreasing the level of neutrophils.

5. Conclusions

In this work, we showed a positive biological effect of TiO_2/316L/1 coatings using *in vitro* and *in vivo* models. Our results indicate that the enhancement of routinely applied in medicine stainless steel 316L with TiO_2/316L/1 layer, may still find wide range of applications in reconstructive medicine. What is more, the present study have demonstrated that

nonaqueous sol-gel method allowed creating a variety of surface modifications of the material, providing the opportunity to find even better solutions in the field of regenerative medicine.

Conflict of Interests

The authors declare that there is no conflict of interests regarding the publication of this paper.

Acknowledgments

The research was partially supported by Wroclaw Research Centre EIT+ under the project "Biotechnologies and Advanced Medical Technologies"—BioMed (POIG.01.01.02-02-003/08) financed from the European Regional Development Fund (Operational Programmed Innovative Economy, 1.1.2.).

References

[1] J. M. Anderson, A. Rodriguez, and D. T. Chang, "Foreign body reaction to biomaterials," *Seminars in Immunology*, vol. 20, no. 2, pp. 86–100, 2008.

[2] D. Buser, B. Hoffmann, J. Bernard, A. Lussi, D. Mettler, and R. K. Schenk, "Evaluation of filling materials in membrane-protected bone defects-a comparative histomorphometric study in the mandible of miniature pigs," *Clinical Oral Implants Research*, vol. 9, no. 3, pp. 137–150, 1998.

[3] K. Gotfredsen, T. Berglundh, and J. Lindhe, "Anchorage of titanium implants with different surface characteristics: an experimental study in rabbits," *Clinical Implant Dentistry and Related Research*, vol. 2, no. 3, pp. 120–128, 2000.

[4] Y. T. Sul, C. Johansson, E. Byon, and T. Albrektsson, "The bone response of oxidized bioactive and non-bioactive titanium implants," *Biomaterials*, vol. 26, no. 33, pp. 6720–6730, 2005.

[5] E. Eisenbarth, "Biomaterials," in *Kirk-Othmer Encyclopedia of Chemical Technology*, Kirk-Othmer, Ed., vol. 7, Wiley-Blackwell, New Jersey, NJ, USA, 2011.

[6] M. Díaz, P. Sevilla, A. M. Galán, G. Escolar, E. Engel, and F. J. Gil, "Evaluation of ion release, cytotoxicity, and platelet adhesion of electrochemical anodized 316 L stainless steel cardiovascular stents," *Journal of Biomedical Materials Research B: Applied Biomaterials*, vol. 87, no. 2, pp. 555–561, 2008.

[7] S. R. Paital and N. B. Dahotre, "Calcium phosphate coatings for bio-implant applications: materials, performance factors, and methodologies," *Materials Science and Engineering R: Reports*, vol. 66, no. 1–3, pp. 1–70, 2009.

[8] A. Simchi, E. Tamjid, F. Pishbin, and A. R. Boccaccini, "Recent progress in inorganic and composite coatings with bactericidal capability for orthopaedic applications," *Nanomedicine: Nanotechnology, Biology, and Medicine*, vol. 7, no. 1, pp. 22–39, 2011.

[9] A. P. Chiriac, I. Neamtu, L. E. Nita, and M. T. Nistor, "Sol gel method performed for biomedical products implementation," *Mini-Reviews in Medicinal Chemistry*, vol. 10, no. 11, pp. 990–1013, 2010.

[10] D. Wang and G. P. Bierwagen, "Sol-gel coatings on metals for corrosion protection," *Progress in Organic Coatings*, vol. 64, no. 4, pp. 327–338, 2009.

[11] S. Oh, C. Daraio, L. Chen, T. R. Pisanic, R. R. Fiñones, and S. Jin, "Significantly accelerated osteoblast cell growth on aligned TiO_2 nanotubes," *Journal of Biomedical Materials Research A*, vol. 78, no. 1, pp. 97–103, 2006.

[12] A. Satsangi, N. Satsangi, R. Glover, R. K. Satsangi, and J. L. Ong, "Osteoblast response to phospholipid modified titanium surface," *Biomaterials*, vol. 24, no. 25, pp. 4585–4589, 2003.

[13] O. V. Salata, "Applications of nanoparticles in biology and medicine," *Journal of Nanobiotechnology*, vol. 2, pp. 1–3, 2004.

[14] T. G. Koch, L. C. Berg, and D. H. Betts, "Current and future regenerative medicine-Principles, concepts, and therapeutic use of stem cell therapy and tissue engineering in equine medicine," *Canadian Veterinary Journal*, vol. 50, no. 2, pp. 155–165, 2009.

[15] M. A. González, E. Gonzalez-Rey, L. Rico, D. Büscher, and M. Delgado, "Adipose-derived mesenchymal stem cells alleviate experimental colitis by inhibiting inflammatory and autoimmune responses," *Gastroenterology*, vol. 136, no. 3, pp. 978–989, 2009.

[16] C. N. Svendsen, "Back to the future: how human induced pluripotent stem cells will transform regenerative medicine," *Human Molecular Genetics*, vol. 15, pp. 32–38, 2013.

[17] C. Nombela-Arrieta, J. Ritz, and L. E. Silberstein, "The elusive nature and function of mesenchymal stem cells," *Nature Reviews Molecular Cell Biology*, vol. 12, no. 2, pp. 126–131, 2011.

[18] P. C. Baer and H. Geiger, "Adipose-derived mesenchymal stromal/stem cells: tissue localization, characterization, and heterogeneity," *Stem Cells International*, vol. 2012, Article ID 812693, 11 pages, 2012.

[19] M. C. Advincula, D. Petersen, F. Rahemtulla, R. Advincula, and J. E. Lemons, "Surface analysis and biocorrosion properties of nanostructured surface sol-gel coatings on Ti6Al4V titanium alloy implants," *Journal of Biomedical Materials Research B: Applied Biomaterials*, vol. 80, no. 1, pp. 107–120, 2007.

[20] A. Shanbhag, H. E. Rubash, and J. J. Jacobs, Eds., *Joint Replacement and Bone Resorption: Pathology, Biomaterials, and Clinical Practice*, Taylor & Francis Group, Boca Raton, Fla, USA, 2006.

[21] T. T. Glant, J. J. Jacobs, G. Molnar, A. S. Shanbhag, M. Valyon, and J. O. Galante, "Bone resorption activity of particulate-stimulated macrophages," *Journal of Bone and Mineral Research*, vol. 8, no. 9, pp. 1071–1079, 1993.

[22] J. Grzesiak, K. Marycz, J. Czogala, K. Wrzeszcz, and J. Nicpon, "Comparison of behavior, morphology and morphometry of equine and canine adipose derived mesenchymal stem cells in culture," *International Journal of Morphology*, vol. 29, no. 3, pp. 1012–1017, 2011.

[23] J. Grzesiak, K. Marycz, K. Wrzeszcz, and J. Czogala, "Isolation and morphological characterisation of ovine adipose-derived mesenchymal stem cells in culture," *International Journal of Stem Cells*, vol. 4, no. 2, pp. 99–104, 2011.

[24] R. H. Lee, B. Kim, I. Choi et al., "Characterization and expression analysis of mesenchymal stem cells from human bone marrow and adipose tissue," *Cellular Physiology and Biochemistry*, vol. 14, no. 4–6, pp. 311–324, 2004.

[25] M. Marędziak, K. Marycz, A. Śmieszek, D. Lewandowski, and N. Y. Toker, "The influence of static magnetic fields on canine and equine stem cells derived from adipose tissue," *In Vitro Cellular & Developmental Biology. Animal*, 2014.

[26] O. D. Schneider, D. Mohn, R. Fuhrer et al., "Biocompatibility and bone formation of flexible, cotton wool-like PLGA/calcium phosphate nanocomposites in sheep," *The Open Orthopaedics Journal*, vol. 5, pp. 63–71, 2011.

[27] T. Kitsugi, T. Nakamura, M. Oka et al., "Bone bonding behavior of titanium and its alloys when coated with titanium oxide (TiO_2) and titanium silicate (Ti5Si3)," *Journal of Biomedical Materials Research*, vol. 32, no. 2, pp. 149–156, 1996.

[28] H. J. Erli, M. Rüger, C. Ragoß et al., "The effect of surface modification of a porous TiO_2/perlite composite on the ingrowth of bone tissue *in vivo*," *Biomaterials*, vol. 27, no. 8, pp. 1270–1276, 2006.

[29] W. Urbański, S. Dragan, E. Gębarowska et al., "Preliminary evaluation of selected biologic properties of TiO_2 and SiO_2 layers on metallic substrates," *Engineering of Biomaterials*, vol. 13, no. 96–98, pp. 129–133, 2010.

[30] S. Kačiulis, G. Mattogno, A. Napoli et al., "Surface analysis of biocompatible coatings on titanium," *Journal of Electron Spectroscopy and Related Phenomena*, vol. 95, no. 1, pp. 61–69, 1998.

[31] J. Gallo, M. Raška, F. Mrázek, and M. Pet'ek, "Bone remodeling, particle disease and individual susceptibility to periprosthetic osteolysis," *Physiological Research*, vol. 57, no. 3, pp. 339–349, 2008.

[32] A. S. Shanbhag, J. J. Jacobs, J. Black, J. O. Galante, and T. T. Glant, "Cellular mediators secreted by interfacial membranes obtained at revision total hip arthroplasty," *Journal of Arthroplasty*, vol. 10, no. 4, pp. 498–506, 1995.

[33] R. Contreras, H. Sahlin, and J. A. Frangos, "Titanate biomaterials with enhanced antiinflammatory properties," *Journal of Biomedical Materials Research A*, vol. 80, no. 2, pp. 480–485, 2007.